JOURNAL OF OPTOELECTRONICS AND ADVANCED MATERIALS Vol. 12, No. 11, November 2010, p. 2199 - 2207

Influence of ethylene glycol on the nanostructured pure and V-doped SnO_2 nanoparticles via sol-gel process and application in photocatalysts

S. GNANAM*, V. RAJENDRAN
Department of physics, Presidency College, Chennai-600 005, Tamilnadu, India

Nanocrystalline ethylene glycol mediated pure and vanadium doped tin oxide (VTO) powders of about 5-20nm in size have been prepared by simple sol-gel method. The molecular structural properties of the prepared pure SnO_2 nanopowders annealed at different temperatures (80-600°C) have been characterized by Fourier transform infrared spectroscopy (FTIR). PL emission spectra show that the introduction of V^{2+} into the SnO_2 host, the defects still play a dominant role with respect to the luminescence processes. The prepared VTO nanoparticles exhibit photocatalytic activity in the degradation of methyl orange, indicating that the SnO_2 nanostructure is promising as a semiconductor photocatalyst.

(Received October 11, 2010; accepted November 19, 2010)

Keywords: Semiconductors; Nanostructured materials; V-SnO_2; Sol-gel process; Photocatalyst

1. Introduction

Nanoscale materials have attracted significantly scientific and industrial due to the fact that they demonstrate a variety of chemical, physical and functional properties different from the corresponding bulk materials. Tin oxide (SnO_2), an n-type semiconductor with a wide band gap (Eg = 3.6 eV at 300 K), is extensively used as a functional material for optoelectronic devices [1], conductive electrodes and transparent coatings due to its good conductivity and transparency in the visible spectrum [2,3], solar cells [4,5], and catalyst support [6]. Tin oxide has been widely used for various electrochemical and catalytic applications, such as solid-state gas sensors for environmental monitoring and active catalyst for partial oxidation and amino oxidation of olefins [7–9]. Many routes have been applied to fabricate nanosized SnO_2 particles, which mainly consist of the sol-gel method [10], solvothermal synthesis [11], spray pyrolysis [12], sonochemical methods [13] and surfactant mediated synthesis [14]. Among various chemical synthesis methods for preparation of metal oxides of large surface area, a sol-gel process offers several advantages over other methods, better homogeneity, controlled stoichiometry, high-purity, phase-pure powders at a lower temperature and flexibility of forming dense monoliths, thin films or nanoparticles. Sol-gel method is widely applied in preparation of nano-SnO_2 powder. Usually, heat post-treatment at high temperature is necessary for removal of organic compounds and to acquire perfect nanocrystalline SnO_2. However, it is very difficult to maintain the nanometric-scale structure of a material when it is subjected to heat-treatments. The heat-treatments steps are fundamental to achieve an optimal combination of mechanical, catalytic and electronic properties [15].

The use of tintetrachloride as precursor and ethylene glycol as solvent overcomes the problems associated with alkoxides. The alcohol (ethylene glycol) itself acts as a stabilizer, limiting particle growth and prohibiting agglomeration. Due to the high temperatures that can be applied (>150°C), often highly crystalline oxides are yielded. Ethylene glycol functions not only as a complexion agent to form a polymeric network but also as a spacer to modulate the distance between metal ions, preventing metal oxides from aggregation during earlier stage of organic removal.

Research has been conducted to improve photocatalytic properties of SnO_2 powders by doping transition metal elements. The photocatalytic activity of semiconductor is due to the production of excited electrons in the conduction band of the semiconductors, along with corresponding positive holes in the valence band under UV illumination. These energetically excited species are mobile and capable of initiating many photocatalytic reactions, usually, by the production of free radical species at the semiconductor surface. They are unstable, however, and the recombination of photo-generated electrons and holes can occur very quickly, dissipating the input energy as heat [16, 17]. With the nanoparticles doped, SnO_2 with transition metal ions would enhance the mobility of exciton, thus facilitating its surface reaction. Although there are plentiful methods to synthesize SnO_2 nanoparticles, little work has been carried out to investigate their photocatalytic behavior so far.

In this work, we report the synthesis of pure and V^{2+}-doped SnO_2 nanoparticles and its application for the photodegradation of aqueous methyl orange for the first time. The introduction of a small quantity of V^{2+} in the reaction system was found to play a great role in the size and shape control. However, with respect to nanocrystalline SnO_2 semiconductor, to the best of our

knowledge, no letter reported on the photocatalytic and luminescent characteristics of VTO nanoparticles. The main purpose of the present research is to study the pre and post-annealing temperature effect on nanoparticle size, nanostructure and optical properties of SnO_2 powders synthesized by the simple sol-gel method.

2. Experimental procedures

All chemical reagents were commercial with AR purity, and used directly without further purification. Initially, a sol solution was prepared by dissolving 11.7ml of tin tetrachloride ($SnCl_4$) in 100ml ethylene glycol ($C_2H_6O_2$) under vigorous stirring at 80°C for 5hrs. Secondly, 0.15g vanadium (III) chloride (VCl_3) was added to the above transparent sol solution. The pH of the sol solution was 1.5, indicating the release of HCl during dissolution of $SnCl_4$. Then it was heated to 120°C for 36 hours to evaporate water and hydrochloride. When the solvent was completely removed, a pale sky-blue colored gel was obtained and it was dried at 150°C for 24hrs. When the pale sky-blue colored gels were dried at 150°C for 6h, 10h and 24hr, it changed into pale brown, dark brown and xerogel respectively. The resultant xerogel was heat-treated at different temperatures from 200-600°C for 2hr. It was found that tinstone begins to form at a temperature as low as 200°C when organics start to burn off. Finally, greenish yellow colored tin oxide nanopowders were formed only after the chemically bonded hydroxyl groups were completely removed at about 600°C. The same procedure was followed by the preparation of pale yellow colored pure tin oxide nanoparticles without addition of dopant.

The XRD pattern of the SnO_2 powder was recorded by using a powder X-ray diffractometer (Schimadzu model: XRD 6000 using CuKα (λ=0.154 nm radiation) with a diffraction angle between 20 and 90º**.** The crystallite size was determined from the broadening of corresponding X-ray spectral peaks by using Debye Scherrer's formula. The Fourier transform infrared (FTIR) spectra of the samples were taken using a FTIR model Bruker IFS 66W Spectrometer. UV-vis absorption spectra of the sample calcined at 600ºC was recorded using a Varian Cary 5E spectrophotometer in the range of 200-800nm (nujol mode). The photoluminescence (PL) spectra of the SnO_2 were recorded by Perkin-Elmer lambda 900 spectrophotometer with a Xe lamp as the excitation light source. Scanning Electron Microscopy (SEM) studies of the SnO_2 were carried out on JEOL, JSM- 67001. Transmission electron microscope (TEM) images were taken using an H-800 TEM (Hitachi, Japan) with an accelerating voltage of 100kV. The specific surface area of the sample was calculated from the formula,

$$S=6x10^3/\rho L$$

where, S is the specific surface area (m^2g^{-1}), L is the average crystallite size, and ρ is the density of the tin oxide.

2.1 Measurement of photocatalytic activity

Methyl orange (MeO), a well-known acid-base indicator, was chosen as a simple model of a series of common azo dyes, largely used in the industry. A photocatalytic experiment was carried out to investigate the photo degradation of methyl orange as a model organic compound. The UV-Vis absorption spectra were obtained on a Perkin Elmer UV-Vis spectrometer RX-1 using water as a solvent in the reference model. The experiment was carried out in a 600ml cylindrical vessel with an 8W mercury vapour lamp (365nm) placed at the axis of the vessel. The lamp was installed in a quartz glass tube to protect it from direct contact with the aqueous solution. Reaction suspensions were prepared by adding 50mg of photocatalyst (Pure and V^{2+}-doped SnO_2 samples calcined at 600ºC for 2h) into the 100ml methyl orange (MeO) solution. The resultant initial concentration of the solution was $3x10^{-3}$ mol/l. Prior to the photodegradation, the suspension was sonicated for 20min and then magnetically stirred in a dark condition for 60 min (initial sample) to establish an adsorption-desorption equilibrium conditions. During UV light irradiation, stirring was maintained to keep the mixture in suspension. At regular intervals, samples were withdrawn and centrifuged to separate SnO_2 particles for analysis. The concentration of methyl orange was analysed by UV-Vis spectrometry at the wavelength 463nm. The photocatalytic efficiency was calculated using the relation $\eta=(1-C_r/C_0)$, where C_0 is the concentration of methyl orange before illumination and C_r is the concentration of methyl orange after a certain irradiation time.

3. Results and discussion

Fig.1A shows the XRD patterns of as-prepared and heat-treated pure SnO_2 powders under different temperatures. All samples (Fig. 1A (b-f) and Fig.1B) present wide diffraction peaks at the same position, which can be indexed to the tetragonal rutile structure of SnO_2 (JCPDS card no.88-0287) with lattice constants of a=4.737 Å and c=3.186 Å. However, the sample of 200ºC (Fig.1A-a) is amorphous, not the tetragonal rutile structure. The crystallization of tin oxide occurs at a temperature 250ºC. No impurity peaks such as vanadium oxide or other tin oxides were observed, indicating that the nanomaterials obtained via our current methods consist of pure phase. The average crystallite sizes of the pure SnO_2 nanocrystals estimated from Debye Scherrer's formula are 5.3, 7.8, 14.1, 17.2 and 20.5nm (250, 300, 400, 500 and 600ºC) respectively, whereas in the case of VTO nanoparticles calcined at 600ºC is 15.1nm. A slight broadening of the peaks is noticed by adding V-dopant in the SnO_2 nanoparticles. From the results, the ethylene glycol mediated VTO SnO_2 nanoparticles were best dispersing and capping ability when compared to pure SnO_2 nanoparticles. Fig.1C shows the variation of the particle size and surface area as a function of the calcination temperature of pure SnO_2 nanoparticles. The effect of the

calcination temperature on the crystallinity and the change in the surface areas of SnO_2 is reported in Table 1.

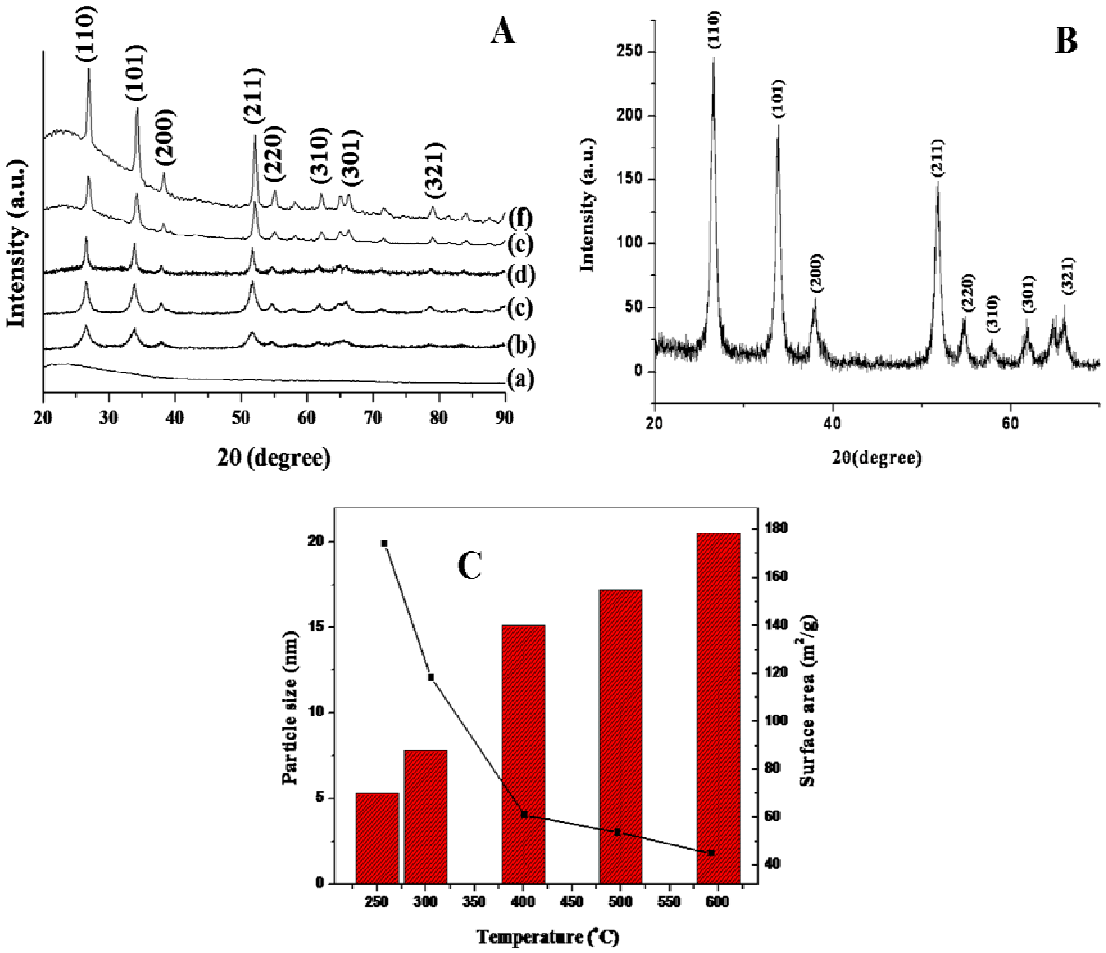

Fig.1A. X-ray diffraction pattern of xerogels at different stage of transition to pure tin oxide (a) 200ºC (b) 250ºC (c) 300ºC (d) 400ºC (e) 500ºC and (f) 600ºC for 2h. Fig.1B V-doped SnO_2 nanoparticles heat-treated at 600ºC for 2h. Fig. 1C. Variation of the particle size and surface area as a function of the calcination temperature of SnO_2.

Table1.XRD and specific surface area results for pure and V^{2+}-doped SnO_2 nanoparticles.

Thermal treatment duration 2h	Particle size D (nm)	Specific surface area S (m^2g^{-1})
250°C	5.3	161.95
300°C	7.8	110.04
400°C	14.1	56.84
500°C	17.2	49.90
Pure SnO_2 600°C	20.5	41.87
V-SnO_2 600°C	15.1	56.84

The FTIR spectra of the sol solution and the gels dried at 150°C for different periods were shown in Fig.2A and 2B. The peaks around 1628 and 3421cm^{-1} correspond to the bending vibrations of absorbed molecular water and the stretching vibrations of –OH groups respectively.

A typical broad band at 3421cm^{-1} indicates that a strong hydrogen bond formed between hydroxyl groups of ethylene glycol. The -O-CH_2-CH_2-O vibration of ethylene glycol gives a sharp intense peak at about 1010cm^{-1}. As expected, the Sn-O terminal mode was not observed in the sol due to the existence of excess ethylene glycol. The degree of aggregation of particles in sol solution plays an important role in colloidal stability, which may further influence the structure of derived gel, the morphology and microstructure of metal oxides during firing. It was noted from Fig.2A and 2B, during drying the peak at around 3400 cm^{-1} becomes smaller and sharper, whereas the intensity of O-C-O mode at 1040cm^{-1} gets stronger.

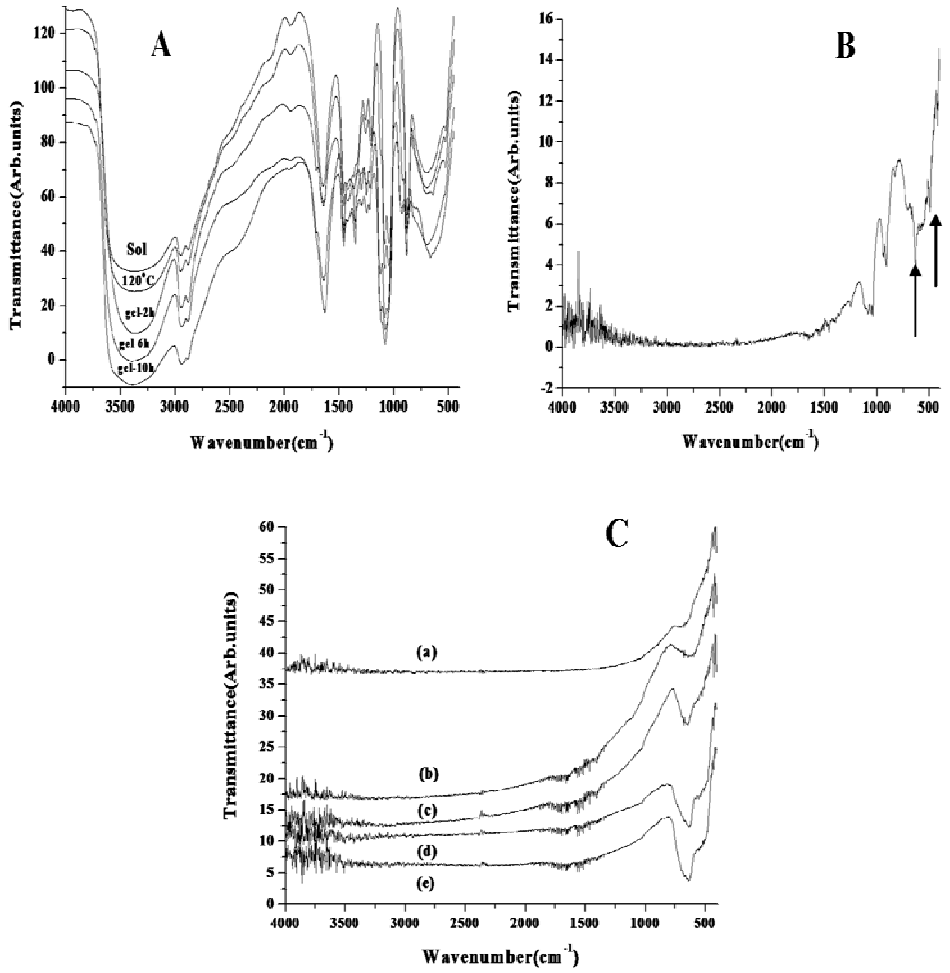

Fig. 2. (2A) FTIR spectra of SnO_2 sol-gel transition (a) a sol solution (b) 120ºC, a gel dried at 150ºC for 2h(c), 6h(d) and 10h(e). (2B) a gel dried at 150ºC for 24h (f). (2C) FTIR spectra of the xerogels heat-treated at different temperatures (a) 200ºC (b)300ºC (c) 400ºC (d) 500ºC and (e) 600ºC for 2h.

These observations confirm that at temperatures ≤ 150°C, the hydrogen bond underwent dehydration and resulted in ester bridge O-C-O, which was one of the mechanisms of the formation of Polymeric network. The bridging (O-Sn-O) and the terminal (Sn-O) modes were observed at 632 and 492cm^{-1} respectively. FTIR spectra of structural evolution of xerogels heat-treated at different temperatures were shown in Fig.2C. Increasing the calcinations temperature results in the decrease in the intensity of water band. The bands at 980 and 1240cm^{-1} are reduced in intensity with increasing temperature. As the broadband in the higher energy region (ca. 3421cm^{-1}) in Fig.2C is completely lost in the spectra, both -O-CH_2-CH_2-O and -OH are expelled during calcination. The ratio remains unity over the temperature range up to 300-600ºC, because the residual organic molecules, which prevent the rearrangement of O-Sn and O-Sn-O bonds. It is interesting to find that the relative intensity of the peak at 632cm^{-1} becomes stronger than that of the one at 492cm^{-1}. However, the peak at 632cm^{-1} is assigned to SnO_2 vibration, which indicates that the products are well crystallized.

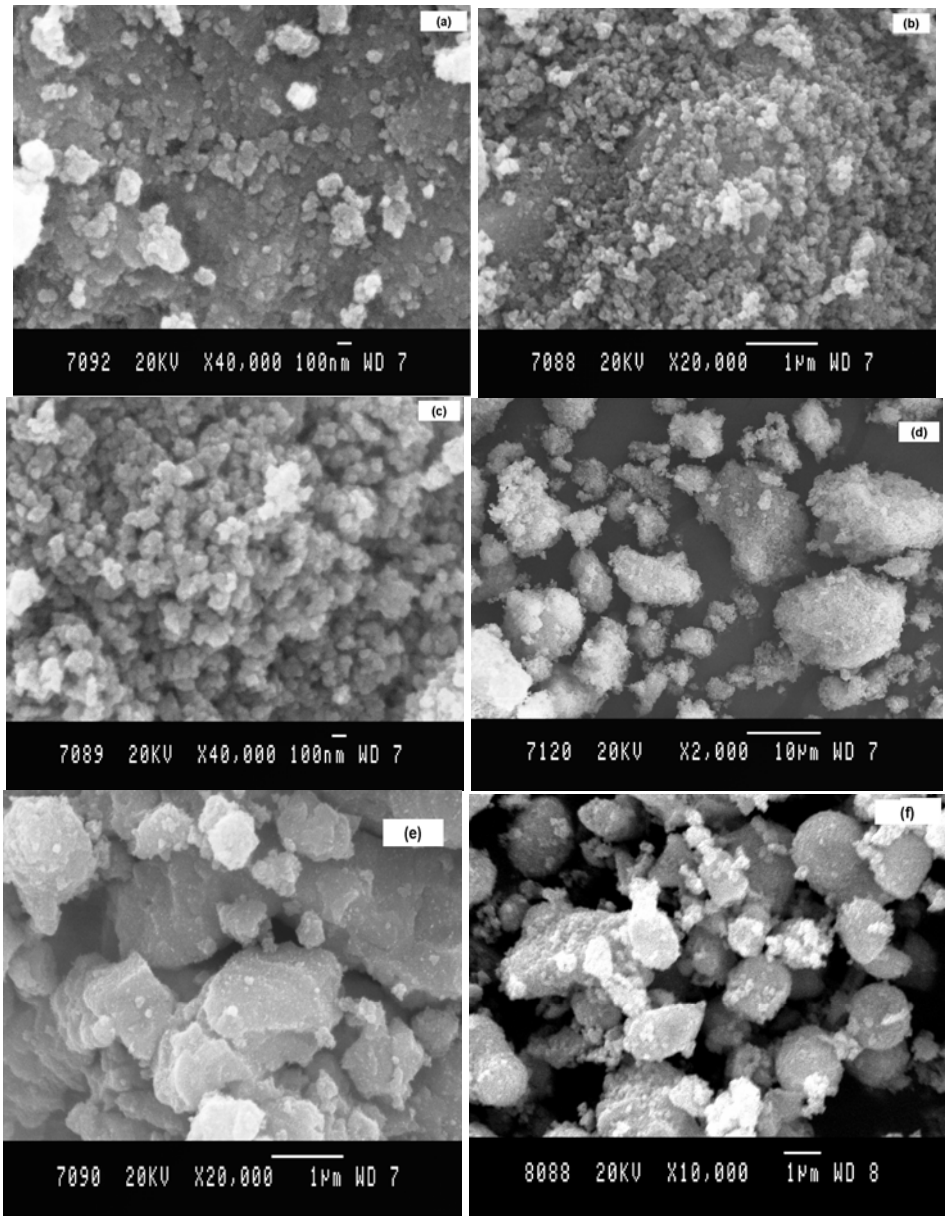

Fig.3 SEM images of the xerogel heat-treated at 250ºC (a), 300ºC (b), 400ºC (c), 500ºC (c) and 600ºC (d) for 2h.
Fig.3e SEM image of V-doped SnO_2 nanoparticles calcined at 600ºC for 2h.

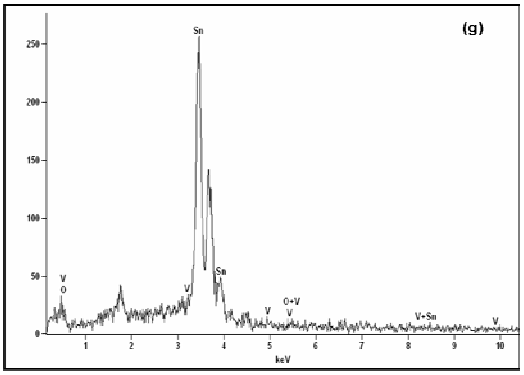

Fig.3g EDX spectrum of V-doped SnO_2 nanoparticles calcined at 600ºC for 2h.

Fig.3A shows the SEM morphology of pure tin oxide particles derived from a gel fired at 250, 300, 400, 500 and 600ºC for 2h. The spherical like morphology of the prepared SnO_2 nanoparticles was shown in Fig.3a-3e. The crystallization of tin oxide occurs at a low temperature and growth continues at high temperatures as the organic groups were removed. The microstructure of the sample synthesized at 250°C is entirely composed of porous shards with agglomerated fine particles (Fig.3a). When the temperature is increased to 300, 400 and 500°C, the sample takes on regular spherecity and the size is very small and uniform ranging as shown in Fig.3 (b-d), which indicates that the as-synthesized SnO_2 crystal grains are well-dispersed. A further increase in temperature (600°C) results in well-crystallized spherical pure tin oxide

nanoparticles (Fig.3e). However, ethylene glycol can offer better viscosity to the medium than other solvents; it can react with $SnCl_4$ more easily to form a polymer network and as a spacer to modulate the distance between tin ions, preventing tin oxide particles from aggregation during earlier stages of organics removal. Fig.3f shows the typical SEM micrograph of VTO nanoparticles derived from a gel calcined at 600°C. Therefore, the appropriate temperature should be 600°C to assure that product has perfect morphology and high purity.

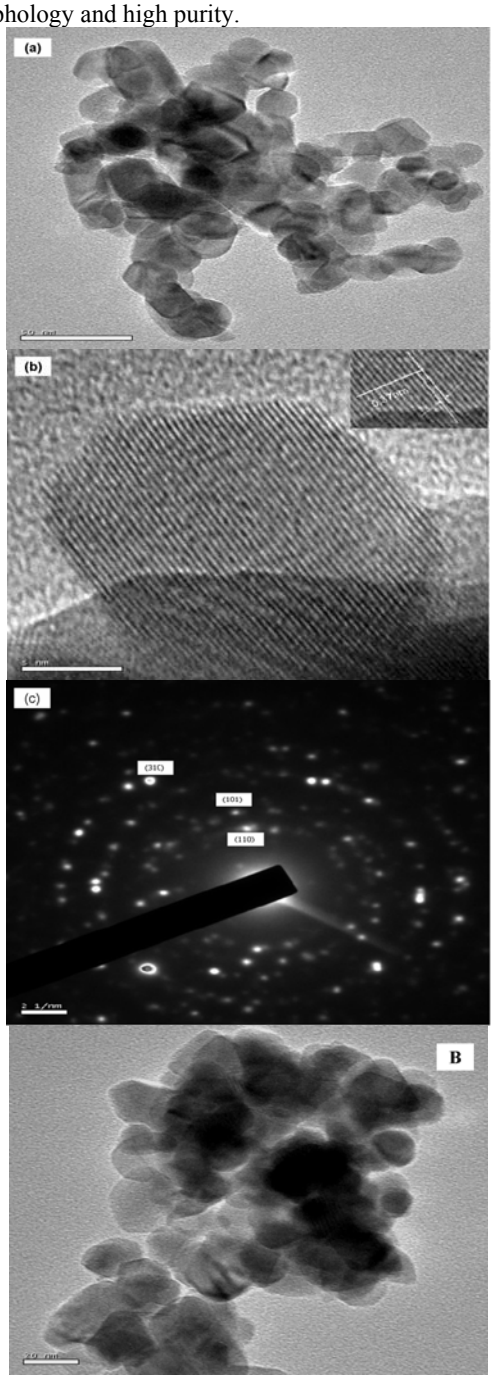

Fig.4B TEM image (a), HR-TEM (b) and SAED (c) pattern of V^{2+}-doped SnO_2 nanoparticles calcined at 600 ºC for 2h. Fig. 4A TEM image of Pure SnO_2 nanoparticles calcined at 600ºC for 2h.

The TEM image, HR-TEM and the selective-area electron diffraction (SAED) pattern of a VTO sample calcined at 600ºC were shown in Fig.4A (a-c). Fig.4a shows the spherical and some hexagonal as morphology of tin oxide nanoparticles derived from a gel fired at 600ºC, for 2h. The average particle size is about 15nm. Most of the nanoparticles were well separated although some of them partially aggregated. Moreover, the particle size of the sample obtained from TEM pattern was quite similar to those calculated from Scherrer's equation. Fig.4b shows the high–resolution TEM (HR-TEM) image of the VTO nanoparticles calcined at 600ºC, for 2h. It shows clear lattice fringes, indicating the established crystallinity of SnO_2 powders. In addition, we know that the lattice images were interference patterns between the direct beam and diffracted beams in HR-TEM and the spacing of a set of fringes is proportional to the lattice spacing, when the corresponding lattice planes meet the Bragg condition. So when we chose an area and magnified for further observation (as shown in the inset of Fig.4b), the distance between lattice fringes was found to be 0.37nm, which was in good agreement with the lattice spacing of (110) plane in the SnO_2. The SAED pattern of the sample shown in Fig.4c distinctly exhibit three diffraction rings which corresponds to the (110), (101), and (301) planes of the tetragonal-phase VTO with cassiterite structure respectively. This is perfectly in agreement with the XRD analytical results, and indicates that the SnO_2 nanoparticles with small average particle sizes were well crystallized. The obvious rings and dots of selective area electron diffraction (SAED) show that poly crystalline nature for the VTO nanocrystals. The TEM micrograph of the pure SnO_2 nanoparticles calcined at 600°C is shown in Fig. 4B. It is clearly observed that the as-prepared SnO_2 nanoparticles are spherical with some aggregated particles, with an average grain size of ~20 nm. This result is similar to that obtained from XRD analysis. The TEM reveals that the doped materials present smaller particle sizes than the pure material, but in both cases, uniform, well-crystallized nanoparticles can be observed. In both the cases, ethylene glycol functions not only as a complexion agent to form a polymeric network but also as a spacer to modulate the distance between tin ions, preventing tin oxide from aggregation during earlier stage of organic removal.

UV-Visible absorption spectrum was recorded in order to characterize the optical absorbance of the nanocrystalline SnO_2. Fig.5a and 5b shows the optical absorbance spectra of the pure and V^{2+}-SnO_2 nanocrystals with photon wavelength in the range of 200–800 nm. The band gap energy (Eg) for the SnO_2 nanocrystallites can be obtained by extrapolation of the rising part to the plot to the X-axis as shown in Fig.5a and 5b. The absorption band edge of the pure and doped samples calcined at 600 ºC, showing obvious blue shift, is estimated around 317nm (3.91eV) and 295nm (4.2eV) respectively, by extrapolating the steep slops in the curve to the long-wavelength side. It reveals that the mean slope of the absorbance of the tin oxide nanoparticles. The obtained values are larger than that of the reported value for bulk SnO_2 (3.6eV) [18], which were also attributed to the

formation of nanocrystalline SnO_2 particles. Considering the blue shift of the absorption positions from the bulk SnO_2, the absorption onsets of the present samples can be assigned to the direct transition of electron in the SnO_2 nanocrystals.

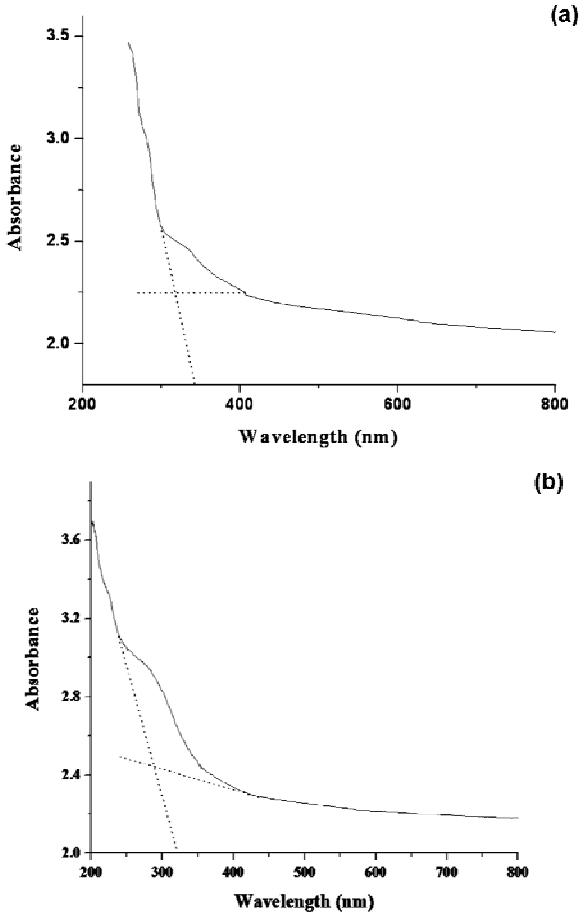

Fig.5. Absorption spectrum of the pure SnO_2 (a) and V^{2+}-doped SnO_2 (b) nanoparticles calcined at 600ºC for 2h.

Fig.6a and 6b shows the PL spectrum of the pure and V^{2+}-doped SnO_2 nanoparticles synthesized in ethylene glycol at 600ºC with an excitation wavelength is 300nm. From Fig.6a, there are about 14 peaks between 400-500nm, it is worth noting that there are seven intense strong emission peaks (398, 413, 440, 451, 467, 482 and 492nm) in the visible emission of 400-500nm. The peak at 559nm was very broad. It was shifted towards the higher wavelength with heat-treatment. It shows that the appearance of emission bands in varying wavelength. Also supports formation of clusters with varying size. Hence, the particles might have varying sizes with different band gap values. It is also supported by TEM analysis as discussed above.

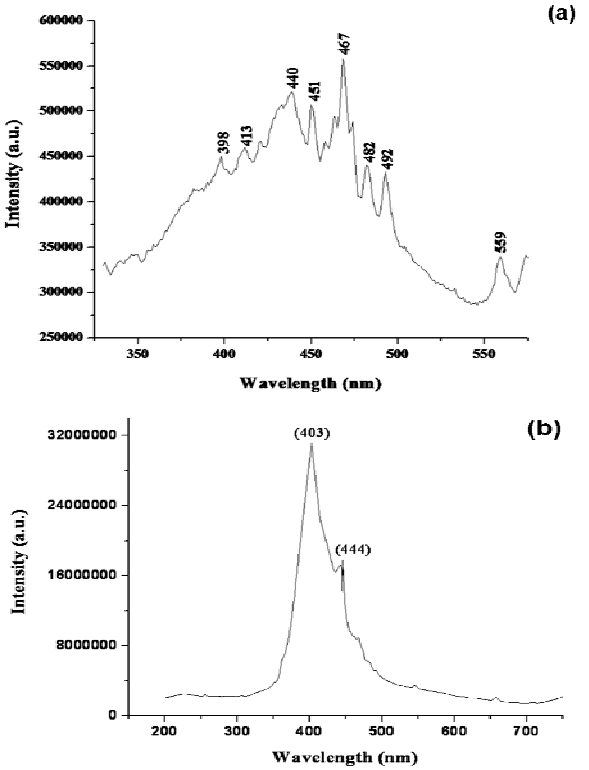

Fig.6. Photoluminescence spectrum of the pure SnO_2 (a) and V^{2+}-doped SnO_2 (b) nanoparticles calcined at 600ºC for 2h.

Distinction between the surface traps and lattice defects is carried out by PL emission study in the pure case, which gives two characteristic peaks at 440 and 467nm respectively. Particularly, the peak position at 467nm is sharp; it is due to the characteristics of the traps present in the nanoparticles [19]. The emission spectrum revealed a blue emission band centred at 440nm, which might be related with oxygen vacancies. This is proved by the fact that the temperature behaviour of luminescence spectra of the nanoscaled SnO_2 powders is similar with those from nanocrystals of $SrTiO_3$, TiO_2, ZnO and $BaTiO_3$ [20-22]. From Fig. 6b, it can be observed that the addition of V^{2+} to SnO_2 host lattice can result in the increment of PL intensity of SnO_2 host, while the characteristic peaks of V^{2+} ions could not be collected. In the V^{2+}-doped SnO_2 nanoparticles, it enhances a very high intense peak located at 403nm in the visible region and also it has one shoulder peak located at 444nm with some very weak emission peaks as shown in Fig.6b. The earlier reports supposed that the intense peak around 400-500nm can be assumed to be due to the formation of a V_o^{++} luminescent center in the SnO_2 nanocrystals and nanorods [23, 24]. In pure SnO_2 host, the emission attributes to electron transition, mediated by defects levels in the band gap, such as oxygen vacancies, tin interstitials and so forth. Doping the tin oxide nanoparticles with transition metal (V^{2+}) significantly improves their optical activity, which may be due to the enhancement of energy transfer. Therefore, it is

of interest to study the role of V^{2+} ion in the SnO_2 host lattice and the contribution to the luminescence.

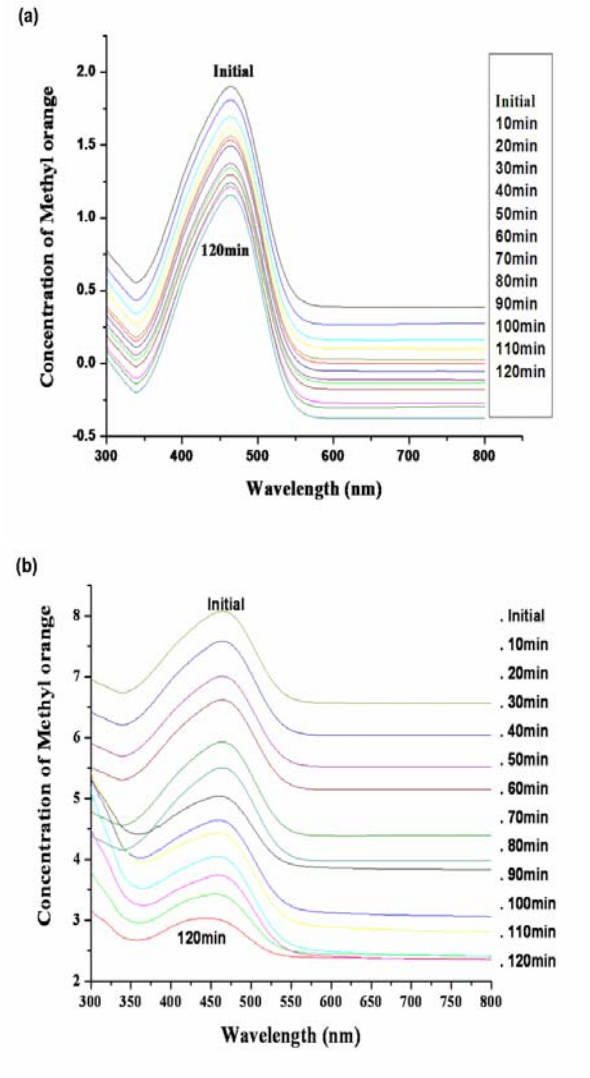

Fig.7. UV-Vis spectra of an aqueous methyl orange sample collected at various irradiation times interval of pure SnO_2 (a) and V^{2+}-doped SnO_2 (b) nanoparticles calcined at 600ºC for 2h.

Photocatalytic activity of SnO_2 nanopowder

In this report, aqueous methyl orange degradation is used to determine the photocatalytic activity of pure and V^{2+}-doped SnO_2 photocatalysts. The UV-Vis spectra of an aqueous methyl orange sample collected at various irradiation time intervals was as shown in Fig.7a and 7b. Steady and small decrease in concentration of methyl orange was observed, as the irradiation time was increased up to 120min in steps of 10min. The absorbance at λ_{max} = 463nm gradually decreases with time. In comparing with UV-Vis characteristic absorption peak of the initial methyl orange solution, the apparent decrease of absorption intensity indicated by the photocatalytic capability of the catalyst to degrade methyl orange. Hence, a material is observed to be phocatalytically active. The photocatalytic activity of pure SnO_2 calcined at 600ºC was investigated and compared with that VTO nanoparticles calcined at 600ºC (Fig.7a and 7b). The photocatalytic activity of VTO was higher than that pure SnO_2. There is nearly lost of MeO at the end of 120min for the dopant catalyst. However, the degradation is only partial at the end of 120min for the pure catalyst. The doping of transition metal significantly enhances the photoactivity for methyl orange reaction, which may be due to the enhancement of energy transfer.

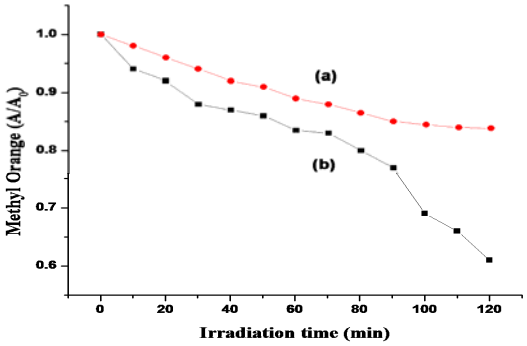

Fig.8. Time course of methyl orange concentration during photodegradation (a) pure SnO_2 and (b) V^{2+}-doped SnO_2 nanoparticles calcined at 600ºC for 2h.

Fig.8 shows the decreasing concentration of MeO versus irradiation time for the samples prepared by sol-gel method. The effect of heat-treatment can be seen, confirming the high photocatalytic activity concluded for the VTO samples treated at 600ºC for 2h. It has small grain size and large specific area and the photoactivities are higher than the pure catalyst calcined at 600ºC. The higher crystallinity combined with good surface state improve the photocatalytic performance. Hence, the photocatalytic degradation of methyl orange indicating that the SnO_2 nanostructure is promising as a semiconductor photocatalyst.

4. Conclusions

Nanocrystalline rutile pure and V^{2+}-doped tin oxide has been successfully prepared by the simple sol-gel route using tin tetrachloride as the precursor and ethylene glycol as the solvent at 600°C. This procedure is straightforward and inexpensive, and consequently can be readily adopted to produce large quantities of nanosized SnO_2 particles. The molecular structures evolutions during the process have been identified using FTIR spectroscopy. The XRD analysis shows that well-crystallized rutile VTO can be obtained and the crystal size was 15.1nm for the sample calcined at 600ºC. The spherical-like morphology of the

prepared SnO_2 nanoparticles was observed from the SEM and TEM studies. Optical measurements show that the VTO nanoparticles generate a visible light emission that may be exploited in gas sensors or other optoelectronic devices. Considering these results, the most suitable annealing temperature for preparation of SnO_2 nanopowder is 600ºC, and the sol-gel method is very efficient for the preparation of homogeneous pure and V^{2+}-doped SnO_2 nanoparticles for nano-sensors, optical, photocatalytic and other industrial applications.

Acknowledgment

The authors are grateful to the University Grand Commission for extending financial assistance to carryout this work and the authors thank Dr.M.Kandasamy and Dr.V.Narayanan, Department of Inorganic chemistry, University of Madras, Chennai-600 0025, for having carried out catalytic studies.

References

[1] D.S. Kumar, P.R. Carbarrocas, J.M. Siefert, Appl. Phys. Lett. **54**, 2088, (1989).
[2] A. Lousa, S. Gimeno, J. Martı, Vacuum **45**, 1143, (1994).
[3] A. Tsunashima, H. Yoshimizu, K. Kodaira, S. Shimada, T. Matsushita, J. Mater. Sci. **21**, 2731 (1986).
[4] S. Ferrere, A. Zaban, B.A. Gregg, J. Phys. Chem. B **101**, 4490 (1997).
[5] Y. Tachibana, K. Hara, S. Takano, K. Sayama, H. Arkawa, Chem. Phys. Lett. **364**, 297, (2002).
[6] D. Wang, S. Wen, J. Chen, S. Zhang, F. Li, Phys. Rev. B **49,** 14282, (1994).
[7] N. Batta, L. Cinquegrani, E. Mugno, A. Tagliente, S. Pizzini, Sensors and Actuators B **6**, 253 (1992).
[8] G. B. Barbi, J. S. Blanco, M. Baroffio, J. Agapito, F. J. Gutierrez, ibid. B **18**, 19 (1994).
[9] K. Wakabayashi, Y. Kamiya, N. Ohta, Bull Chem. Soc. Jpn. **40**, 2127 (1967).
[10] V. Briois, M. Belin, M. Z. Chalaca, R. H. A. Santos, C. V. Santilli, S. H. Pulcinelli, Chem. Mater. **16**, 3885 (2004).
[11] T. Moon, C. Kim, S. Hwang, B. Park, Electrochem. Solid State Lett. A **9** 408 (2006).
[12] J. Pena, J. Perez-Pariente, M. Vallet-Regi, J. Mater. Chem. **13**, 2290 (2003).
[13] J. Zhu, Z. Lu, S. T. Aruna, D. Aurbach, A. Gedanken, Chem. Mater. **12**, 2557 (2000).
[14] D. Chen, L. Gao, J. Colloid Interf. Sci. **279**, 137 (2004).
[15] F. Sala, F. Trifiro, J. Catal. **34**, 68, (1974).
[16] J. Ovenstone, J. Mater. Sci. **36**, 1325 (2001).
[17] J. G. Yu, X. J. Zhao, J. C. Du, W. M. Chen, J. Sol-Gel Sci. Technol. **17**, 163 (2000).
[18] Raghumani Singh Ningthoujam, S.K. Kulshreshtha, J. Mat. Res. Bulltetin. **6**, 4147, (2008).
[19] V. Zhang, M. S. Zhang, Z. Yin, Q. Chen, Appl. Phys. B **70**, 261 (2000).
[20] W. F. Zhang, M. S. Zhang, Z. Yin, Phys. Stat. Sol. **179**, 319 (2000).
[21] D. W. Bahnemann, C. Kormann, M. R. Hoffmann, J. Phys. Chem. **91**, 3789 (1987).
[22] Y. Wang, N. Herron, J. Phys. Chem. **95**, 525 (1991).
[23] K. Vanheusdan, W. L. Warren, C. H. Seager, D. R. Tallant, J. A. Voigt, B. E. Gnade, J. Appl. Phys. **79**, 7983 (1996).
[24] B. Cheng, J. M. Russell, W. Shi, L. Zhang, E. T. Samulski, J. Am. Chem. Soc. **126**, 5972 (2004).

*Corresponding author: gnanam.sambatham@gmail.com